Electrochimica Acta 137 (2014) 758–766

Contents lists available at ScienceDirect

Electrochimica Acta

journal homepage: www.elsevier.com/locate/electacta

The effect of a perpendicular and cumulative inlet flow on the mass-transfer distribution in parallel-plate electrochemical reactors

A.N. Colli, J.M. Bisang*

Programa de Electroquímica Aplicada e Ingeniería Electroquímica (PRELINE), Facultad de Ingeniería Química, Universidad Nacional del Litoral, Santiago del Estero 2829, S3000AOM Santa Fe, Argentina

ARTICLE INFO

Article history:
Received 14 March 2014
Received in revised form 21 May 2014
Accepted 10 June 2014
Available online 17 June 2014

Keywords:
Current distribution
Electrochemical reactors
Hydrodynamic behaviour
Mass-transfer coefficient
Parallel-plate electrodes

ABSTRACT

A perpendicular inlet flow of electrolyte is analysed as a means of improving mass-transfer in a parallel-plate electrochemical reactor. Experimental local Sherwood numbers along the electrode length are reported for different values of the hydraulic diameter and Reynolds number, using the reduction of ferricyanide as a test reaction. The Reynolds numbers, evaluated with the inlet velocity in the reactor, range from 0.7 to 30 with interelectrode gaps varying between 3.2 to 9.8 mm. The perpendicular and cumulative flow makes uniform the mass-transfer distribution at the reactor inlet under laminar flow conditions. The experimental data are compared with theoretical calculations obtained by computational fluid dynamics and also with an analytical simplified model. The mean relative deviation between the experimental and theoretical results was lower than 5% and a close agreement was observed between both theoretical treatments.

1. Introduction

In the industrial practice the mass-transfer has a crucial influence on the performance of the equipments. The improvement of the efficiency of electrochemical reactors requires to increase the mean mass-transfer coefficient and also to become more uniform the mass-transfer distribution along the electrode length. Additionally, in the case of parallel-plate electrodes the behaviour is affected by the entrance and exit effects, which involves an appropriate design of the ports for the inlet and outlet of the electrolyte to the reactor [1]. To address the above issues different alternatives are proposed: (i) placing obstacles in the interelectrode gap to promote turbulence [2], increasing the roughness of the electrode [3] and (iii) sparging a gas in the interelectrode gap or its evolution at the electrode surface [4], which were previously discussed [5]. Other strategy is the modification of specific hydrodynamic aspects of the reactor. Thus, several studies have been devoted to the investigation of different patterns for the flow of the electrolyte inside the equipment. The effect of the geometrical parameters of multijets of electrolyte on the overall mass-transfer behaviour at a flat circular electrode was investigated and a satisfactory empirical correlation of the results was reported [6,7]. Oren et al. [8] analysed the interaction over a flat electrode of two identical solutions jets entering an electrochemical reactor in opposite directions, on the same axis, and leaving it in a direction perpendicular to the inlet flow. This concept, also called impinging streams, has shown only a slight improvement of the mean mass-transfer coefficient. However, the dimensionless ratio of the mass-transfer coefficient to the energy consumption exhibits a better performance in comparison with the single stream mode. Reade et al. [9] studied the effect of a jet flow of electrolyte on the performance of a reticulated vitreous carbon rotating cylinder electrode. The electrolyte jet impinged on the bottom central part of the electrode in line with the rotation axis producing an enhancement in the mass-transfer coefficient between 3–46% depending on the rotation speed and type of electrode material.

Legentilhomme and Legrand [10] studied the mass-transfer characteristics at the inner electrode of an annulus in laminar and turbulent swirling flows induced by means of a tangential inlet in the annular gap. Enhancement of the mean mass-transfer coefficient up to 400% was achieved in comparison to that obtained in fully developed axial flow. This concept was also implemented for the cathodic removal of metal from dilute process solutions [11]. Recently, Martínez-Delgadillo et al. [12] evaluated, using computational fluid dynamics, three different inlet types of a tubular electrochemical reactor and it was found that axial velocity distribution is more homogeneous when the reactor is operated with a tangential inlet.

* Corresponding author.
E-mail address: jbisang@fiq.unl.edu.ar (J.M. Bisang).

http://dx.doi.org/10.1016/j.electacta.2014.06.061
0013-4686/

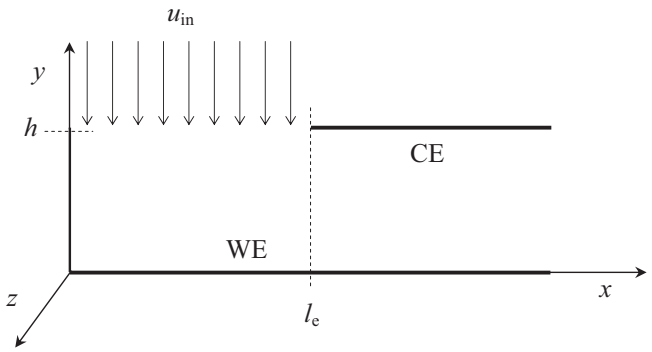

Fig. 1. Schematic view of the reactor with perpendicular inlet flow and coordinates. WE, working electrode; CE, counter electrode.

Cœuret and Legrand [13] proposed the 'falling-film cell', a parallel-plate electrochemical reactor where a gravity flow of electrolyte occurs over an inclined plate and below a sheet of expanded metal positioned above and parallel to the plate. At low flow rates capillary effects are present producing an increase in the mass-transfer coefficient when the flow rate is decreased, called capillary flow regime, which was industrially implemented for the removal of metal ions from effluents.

The use of a pulsed flow reactor was analysed to enhance mass-transfer at the electrode [14], pulsation induces stirring of the electrolyte which is easily controlled by the amplitude and frequency of the pulse. This concept was primarily developed at commercial scale for metal recovery in wastewaters and also for electroorganic synthesis.

In a previous paper from this laboratory [5], a continuous reduction in the cross-section area was analysed as a means of improving mass-transfer in a parallel-plate electrochemical reactor. Thus, it was achieved a convergent flow along the reactor, which improved the mass-transfer coefficient by 10-60% and the mass-transfer distribution under laminar flow conditions was more uniform.

Jorne [15] and Lessner and Newman [16] investigated a cumulative flow channel in which the electrolyte was uniformly fed through a porous wall facing the active electrode. Because of the cumulative nature of the flow, the average velocity increases linearly along the length of the electrode and the diffusion boundary layer becomes uniform. This arrangement is a unique flow system that exhibits uniform accessibility to mass transfer. The concept was applied to the case of a zinc-chloride battery [17]. However, its implementation is difficult in the case of parallel-plate electrochemical reactors when both electrodes are massive.

The aim of this paper is to study in electrochemical reactors with parallel-plate electrodes the effect of a perpendicular inlet flow on the mass-transfer distribution. Thus, the fluid is fed uniformly through a port facing the electrode. The port has the same width as the electrode and the end of the channel is closed off. Because of the cumulative nature of the flow the average velocity increases linearly along the length of the port and the electrode is uniformly accessible to mass-transfer.

2. Mathematical modelling of the mass transfer

Figure 1 sketches the modelled electrochemical system, consisting of a rectangular flow channel where one wall is the working electrode facing the counter electrode that covers partially the opposite wall. Thus, at $y = h$ for $0 \le x \le l_e$ the electrolyte is uniformly fed and in this region the flow is cumulative. For a parallel-plate electrochemical reactor the distribution of the local Sherwood number, Sh_x, along the electrode length is given by [18]

$$Sh_x = \frac{\sqrt{\varepsilon}}{\Gamma(4/3)}\left(\frac{Re_{in}Sc}{9\int_0^X \sqrt{\varepsilon}dX}\right)^{1/3} \quad (1)$$

being

$$\varepsilon = \left.\frac{\partial U_X}{\partial Y}\right|_{Y=0} \quad (2)$$

$$U_X = \frac{u_x}{u_{in}} \quad (3)$$

$$X = \frac{x}{d_h} \quad (4)$$

and

$$Y = \frac{y}{d_h} \quad (5)$$

where the local Sherwood number, Sh_x, the Reynolds number, Re_{in}, and the Schmidt number, Sc, are defined as

$$Sh_x = \frac{k_{m,x}d_h}{D} \quad (6)$$

$$Re_{in} = \frac{u_{in}d_h}{\nu} \quad (7)$$

and

$$Sc = \frac{\nu}{D} \quad (8)$$

here $k_{m,x}$ is the local mass-transfer coefficient, d_h is the hydraulic diameter, ν is the kinematic viscosity, D is the diffusion coefficient and u_{in} is the average fluid velocity at the reactor inlet.

The hydrodynamic regime inside the reactor in steady-state is given by the Navier-Stokes equations

$$U_X\frac{\partial U_X}{\partial X} + U_Y\frac{\partial U_X}{\partial Y} = -\frac{\partial P}{\partial X} + \frac{1}{Re_{in}}\left[\frac{\partial^2 U_X}{\partial X^2} + \frac{\partial^2 U_X}{\partial Y^2}\right] \quad (9)$$

$$U_X\frac{\partial U_Y}{\partial X} + U_Y\frac{\partial U_Y}{\partial Y} = -\frac{\partial P}{\partial Y} + \frac{1}{Re_{in}}\left[\frac{\partial^2 U_Y}{\partial X^2} + \frac{\partial^2 U_Y}{\partial Y^2}\right] \quad (10)$$

Thus, to calculate the local Sherwood number it is necessary to introduce into Eq. (1) the function ε, which requires the simultaneous solution of Eqs. (9) and (10) together with the continuity equation

$$\frac{\partial U_X}{\partial X} + \frac{\partial U_Y}{\partial Y} = 0 \quad (11)$$

being

$$U_Y = \frac{u_y}{u_{in}} \quad (12)$$

where u_x and u_y are the velocities of fluid along the axial coordinates and P is the dimensionless pressure. The variation of the local Sherwood number along the electrode width can be disregarded due to the small ratio between the interelectrode gap and the electrode width [5,19].

Assuming that at the entrance region the velocity component in the y direction is not a function of x, that is

$$U_Y = -\Theta(Y) \quad (13)$$

Eqs. (9-11) are simplified to the following ordinary differential equation [15,16,20]

$$\frac{d\Theta}{dY}\frac{d^2\Theta}{dY^2} - \Theta\frac{d^3\Theta}{dY^3} = \frac{1}{Re}\frac{d^4\Theta}{dY^4} \quad (14)$$

with the boundary conditions

$$\text{at} \quad Y = 0 \quad \Theta = 0 \quad \text{and} \quad \frac{d\Theta}{dY} = 0 \tag{15}$$

$$\text{at} \quad Y = \frac{1}{2} \quad \Theta = 1 \quad \text{and} \quad \frac{d\Theta}{dY} = 0 \tag{16}$$

Thus, for $0 \le x < l_e$, combining Eqs. (11) and (13) with Eq. (2) results in

$$\varepsilon = X \left.\frac{d^2\Theta}{dY^2}\right|_{Y=0} = X\Theta''(0) \tag{17}$$

Introducing Eq. (17) into Eq. (1) and rearranging yields

$$Sh_x = 0.616\left[Re_{in} Sc \Theta''(0)\right]^{1/3} \quad \text{for} \quad 0 \le x < l_e \tag{18}$$

Furthermore, for $x \ge l_e$ it is assumed that the laminar flow is fully developed. Then [18]

$$\varepsilon = 12\frac{l_e}{h} \tag{19}$$

where l_e is the length of the entrance region and h the interelectrode gap. Introducing Eqs. (17) and (19) into Eq. (1) and rearranging results in

$$Sh_x = 2.0924\left[\frac{Re_{in}\ \ Sc}{\sqrt{\Theta''(0)}/3 + \sqrt{6}(X^+ - 1)}\right]^{1/3} \quad \text{for} \quad x \ge l_e \tag{20}$$

being

$$X^+ = \frac{x}{l_e} \tag{21}$$

Combining Eqs. (18) and (20), the local Sherwood number along the total electrode length can be expressed by

$$Sh_x\, Sc^{-1/3} = [1 - H(X^+ - 1)]\,0.616\left[Re_{in}\Theta''(0)\right]^{1/3} + \\ + H(X^+ - 1)\,2.092\left[\frac{Re_{in}}{\sqrt{\Theta''(0)}/3 + \sqrt{6}(X^+ - 1)}\right]^{1/3} \tag{22}$$

where H is the Heaviside shifting function defined as

$$H(X^+ - 1) = 0 \quad \text{for} \quad X^+ < 1 \tag{23}$$

$$H(X^+ - 1) = 0 \quad \text{for} \quad X^+ \ge 1 \tag{24}$$

3. Experimental

The determination of mass-transfer distribution was performed in an electrochemical reactor with parallel-plate electrodes, as shown in Fig. 2. The anode, a nickel sheet of 80 mm wide, 96 mm long and 1 mm thick, was electrically fed along its middle part by means of a copper current feeder, which was connected to the dc power supply at both ends to ensure isopotentiality of the metal phase. The segmented cathode, 80 mm wide and 136 mm long, was made using a standard printed circuit board technique. A copper clad board was masked with stickers simulating the segments and the copper between them was dissolved by means of a ferric chloride solution at 50 °C during 20 minutes. Then, the stickers were mechanically removed and the segmented copper board was washed with trichloroethylene and acetone and plated with nickel from a conventional Watts type bath [21]. The thickness of the nickel coating was 50 μm. Calibrated resistors, 6.8 Ω resistance, were welded between each segment and the cathodic current feeder, which was electrically connected at both ends. The effect of the calibrated resistors on the current distribution can be neglected due to the small value of their ohmic drop, approximately 10 mV, in comparison with the other terms of the voltage balance in the reactor. The length of the segments and the insulating insertions between them is a critical factor in the design of the equipment in order to obtain accurate experimental results and their dimensions represent a compromise between opposite effects. Thus, the use of a segmented electrode allows to calculate the mean mass-transfer coefficient at each segment, which approaches the local value when smaller is the size of the segment. However, a very small segment drains low current, making difficult its measurement in the calibrated resistor. In Fig. 2, part (b), it is sketched the segmented cathode, which presents 36 segments showing symmetry with respect to the entrance and exit regions. Thus, the first ten segments have 2.5 mm long, followed by 4 segments of 4 mm long and 4 central segments of 4.5 mm long with an insulating region between them of 0.5 mm. The smallest segments at the entrance and exit regions pretend to obtain more experimental results in the electrode section where the effect of the perpendicular flow is expected to be pronounced. Likewise, the insulating insertions between segments disturb the concentration profiles at the electrode surface [22] altering the mass-transfer behaviour. To check this influence, additional calculations using computational fluid dynamics were performed considering two geometric configurations: (i) a segmented cathode with insulating insertions between the segments and (ii) a massive cathode without segments. The mean mass-transfer coefficient at each segment was calculated and compared with the mean value of the same region in the massive electrode. The difference between both mean values can be attributed to the effect of the insulating region between segments. Thus, it was shown that the maximum error in the measurement of the mass-transfer coefficient, as a result of the use of a segmented electrode, may be in the order of 14%, which is an acceptable value for this type of experiments.

By measuring the ohmic drop in the resistors, it was possible to determine the axial current distribution and to calculate the mass-transfer coefficient at each segment, $k_{m,s}$, according to

$$k_{m,s} = \frac{I_{lim}}{\nu_e F W l c} \tag{25}$$

which approaches the local value, $k_{m,x}$. Here I_{lim} is the limiting current at each segment, l is the segment length, W is the segment active width, ν_e is the number of electrons interchanged F is the Faraday constant and c is the bulk concentration of the electroactive species. Data acquisition was performed simultaneously in all segments using a computer controlled, home made analogue multiplexer.

The lower and upper parts of the reactor present perpendicular chambers for the inlet and outlet of the electrolyte, 80 mm wide and 20 mm long. The chambers, showed in Fig. 2, part (c), were filled in the upper part with glass beads, 4 mm diameter, with a plastic foam layer at the lower part. Thus, a uniform distribution of electrolyte is achieved in the plane of the counter electrode, for $0 \le x \le l_e$, to obtain a cumulative flow in this region. Four interelectrode gaps were used, 3.2, 5.4, 7.6 and 9.8 mm, which were fixed by the thickness of the gasket. The reactor was made part of a flow circuit system consisting of a pump, a flow meter, a reservoir and connections to maintain the temperature at the preset value, 30 °C.

The test reaction was the electrochemical reduction of ferricyanide from solutions with $[K_3Fe(CN)_6] \cong 0.01$ mol dm^{-3}, $[K_4Fe(CN)_6] \cong 0.01$ mol dm^{-3}, in 0.65 mol dm^{-3} of K_2CO_3 as supporting electrolyte [18,23], while the reverse reaction occurred at the anode. Table 1 summarizes the composition and physicochemical properties of the solution. Samples of the solution were taken from the reservoir after each experiment and the ferricyanide concentration was spectrophotometrically determined. Nitrogen was bubbled in the reservoir for 1 h prior to the experiment in order to remove the dissolved oxygen. The experiments were

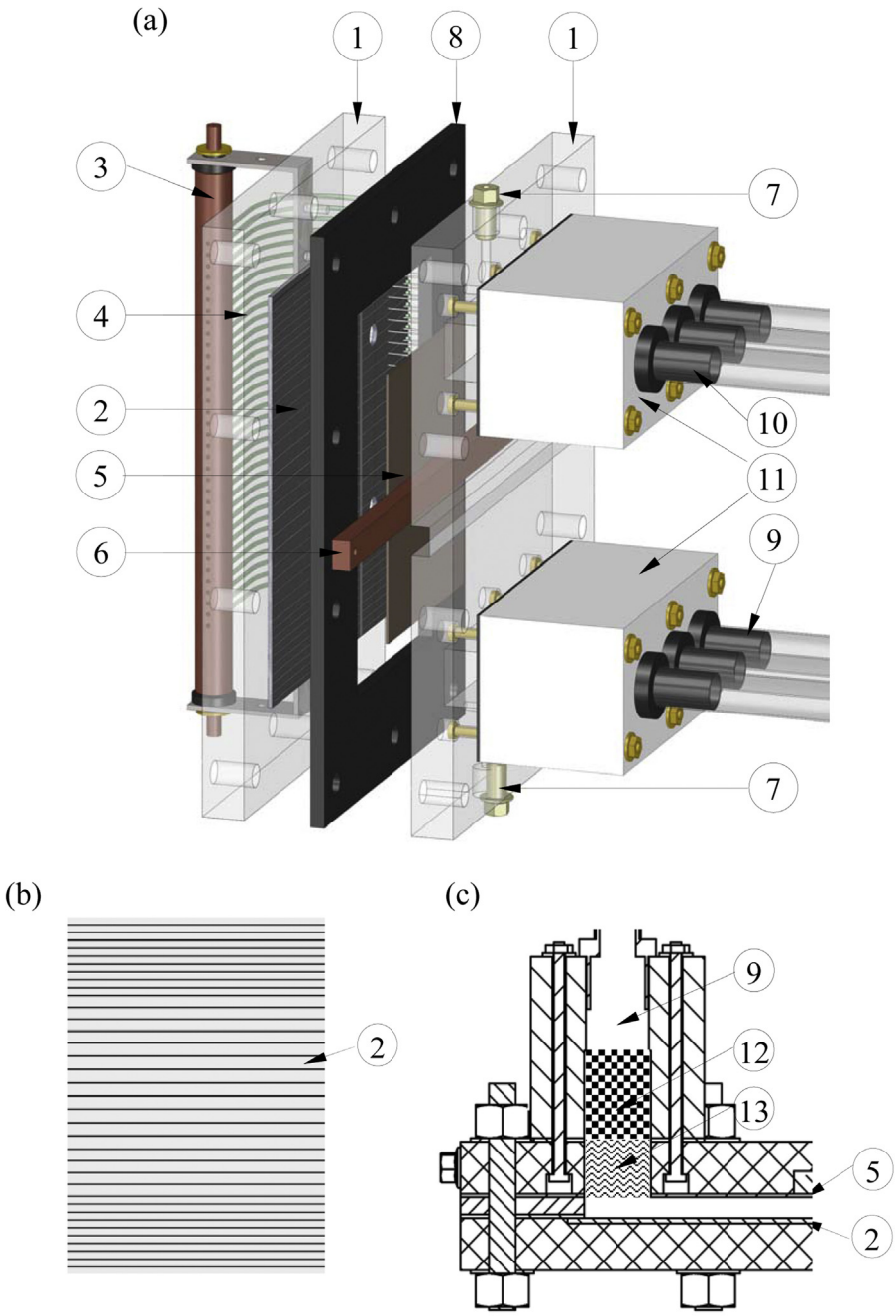

Fig. 2. (a) Schematic representation of the parallel plate electrochemical reactor. (b) View of the segmented electrode. (c) Cross-section showing the electrolyte inlet chamber in the reactor. (1) plates; (2) segmented electrodes; (3) current feeder to the working electrode; (4) calibrated resistors; (5) counter electrode; (6) electrical connection to the counter electrode; (7) Luggin capillaries; (8) gasket; (9) electrolyte inlet; (10) electrolyte outlet; (11) electrolyte distribution chambers; (12) glass beads; (13) plastic foam.

Table 1
Properties of the electrolyte.

Composition	$[K_3Fe(CN)_6] = 0.01$ M $[K_4Fe(CN)_6] = 0.01$ M $[K_2CO_3] = 0.65$ M
Kinematic viscosity (m^2/s)	1.31×10^{-6}
Diffusion coefficient (m^2/s)	8.10×10^{-10}
Sc	1617
ν_e	1

carried out potentiostatically at −0.3 V, the cathodic potential was controlled against a saturated calomel electrode connected to a Haber-Luggin capillary positioned at one end of the cathode. However, the cathodic potential was also measured at the other end of the cathode in order to ensure that all the segments were under limiting current conditions.

4. Results and discussion

4.1. Hydrodynamic calculations

The velocity profiles inside the reactor were calculated using a routine written in Matlab for a rectangular region [18], by solving numerically in laminar flow the Navier-Stokes equations together with the continuity equation. These calculations were also corroborated by means of the OpenFOAM free software, with the use of the simpleFoam routine. At the reactor inlet it was assumed that

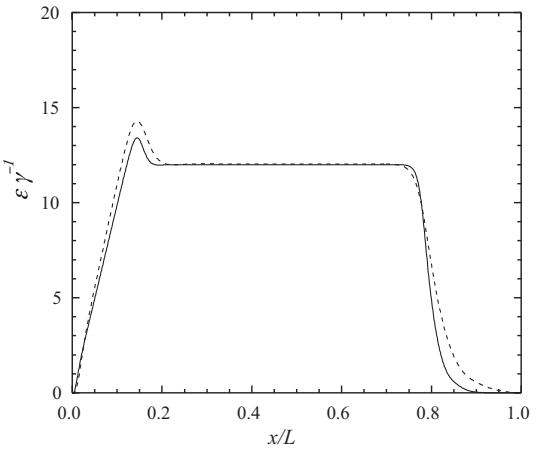

Fig. 3. Slope in the velocity profile at the electrode surface as a function of the dimensionless axial position along the reactor according to the numerical solutions of the Navier-Stokes equations. Full lines: d_h = 6.4 mm, Re_{in} = 5.5. Dashed lines: d_h = 10.8 mm, Re_{in} = 9.35.

the velocity profile is uniform and the gradient of pressure is zero. On the other hand, at the reactor outlet it was considered that the velocity gradient is zero whereas the pressure is uniform. A non-slip boundary condition was used at the solid walls. The absolute tolerances for the calculation of velocity and pressure profiles were 1×10^{-5} and 1×10^{-6}, respectively. The relaxation factor was set to 0.3 for pressure and 0.7 for velocity. The computational region was divided into 650 by 150 structured meshes in the *x*-*y* directions, respectively. A non-uniform mesh grading was used for the mesh size in the *y* direction, Δy, which was gradually varied according to a geometric progression with a ratio of 5 between the size of the last and the first cell. For the smallest cells, at the electrode surface, it was $\Delta y = 8.5 \times 10^{-6}$ m and 2.6×10^{-5} m for d_h = 6.4 mm and d_h = 19.6 mm, respectively. The independence of the results on the grid size was checked. Details and justification of the procedure were given in our previous paper [5]. Likewise, Eq. (14) together with the boundary conditions, Eqs. (15) and (16), were numerically solved. Fig. 3 shows typical curves of the slope in the velocity profile at the electrode surface, ε, along the entire electrode length, *L*, according to the numerical solution of the Navier-Stokes equations, where the aspect ratio γ is defined as

$$\gamma = \frac{l_e}{h} \tag{26}$$

It is observed a linear increase of ε, in the region of the reactor inlet, as expected ε/γ approaches 12 when the flow is developed and a pronounced decay of the velocity profile takes place at the end of the electrode, showing that a perpendicular flow is not convenient at the reactor outlet. For this reason the following figure will be focussed on the inlet and central parts of the reactor. Fig. 4 compares ε according to the numerical solution of the Navier-Stokes equations, full lines, with the values given by Eq. (14), dashed lines, for different values of the Reynolds numbers and γ, where a good agreement is observed between them in the middle range of X^+, and the agreement is increased for higher values of γ. Additionally, the inset illustrates about the slope in the velocity profile at the counter electrode surface. Likewise, ε/γ approaches 12 for high values of X^+ at both electrodes, which validates the assumption given by Eq. (19). Moreover, Fig. 5 shows, as a function of the Reynolds number, the X^+_{Crit}, defined as the X^+ value for which the relative deviation of ε between the prediction according to the Navier-Stokes equations and that given by Eq. (17) is 2%. From Fig. 5 it can be concluded that at low values of X^+, lower part in Fig. 5, the deviations between the rigorous and simplified treatments only depend on the aspect ratio γ, being independent on the Reynolds number. However, when X^+ approaches the unity, upper part in Fig. 5, the deviations depend on both γ and Reynolds number. From Figs. 4 and 5 it can be concluded that for γ higher than 3 there is a close agreement between the behaviour of the models. Then, for simplicity, ε can be evaluated introducing in Eq. (17) $\Theta''(0)$ obtained from the resolution of Eq. (14).

Fig. 6 shows $\Theta''(0)$ as a function of the Reynolds number. The points correspond to the numerical solution of Eq. (14) together with the boundary conditions given by Eqs. (15) and (16). The full lines in Fig. 6 represent limiting behaviours of $\Theta''(0)$ according to the following Eqs. [15,16,24]

$$\Theta''(0) = 24 + \frac{32}{35}Re_{in} \quad \text{for} \quad Re_{in} \le 8 \tag{27}$$

$$\Theta''(0) = 26 + \frac{7}{10}Re_{in} \quad \text{for} \quad 8 < Re_{in} < 30 \tag{28}$$

$$\Theta''(0) = 9.82(Re_{in})^{0.45} \quad \text{for} \quad 30 < Re_{in} < 680 \tag{29}$$

$$\Theta''(0) = 6.88(Re_{in})^{0.5} \quad \text{for} \quad Re_{in} \ge 680 \tag{30}$$

The vertical dashed lines show the validity range for each equation. The comparison of the ε value taking into account Eqs. (27) to (30) with that according to the numerical solution of Eq. (14) gives an error of 1% for Eq. (27), 2% for Eqs. (28) and (29) and 4% when Eq. (30) is used. From Fig. 6 it can be concluded that for reactors with an aspect ratio γ higher than 3, Eqs. (27) to (30) can be introduced into Eq. (17) for the evaluation of ε with an acceptable error in the calculations, instead of the numerical solution of the Navier-Stokes equations.

4.2. Primary current distribution

The primary potential distribution was obtained by solving the Laplace equation in the solution phase including the chamber for the inlet of electrolyte:

$$\frac{\partial^2\phi(x,y)}{\partial x^2} + \frac{\partial^2\phi(x,y)}{\partial y^2} = 0 \tag{31}$$

where ϕ is the potential in the solution phase. For symmetry, only half of the reactor was considered and the current distribution in the direction of the electrode width, *z* coordinate in Fig. 1, was neglected. Eq. (31) was numerically solved by using the finite difference method with an equidistant grid and taking into account the following boundary conditions:

$$\phi = U_A \tag{32}$$

$$\phi = U_C \tag{33}$$

being U_A and U_C the potentials in the solution phase adjacent to the terminal anode and cathode, respectively.

At the insulating walls is:

$$\left.\frac{\partial\phi}{\partial p}\right|_{\text{insulating walls}} = 0 \tag{34}$$

p being the perpendicular coordinate to the wall. Likewise, at each electrode surface the local current density, *j*, can be calculated as

$$j_k = -\frac{1}{\rho}\left.\frac{\partial\phi}{\partial y}\right|_{\text{k th electrode surface}} \tag{35}$$

here k denotes the anode or the cathode and ρ is the electrolyte resistivity.

The solution of the above equations was performed with a home-made routine utilizing the scientific computing platform Matlab.

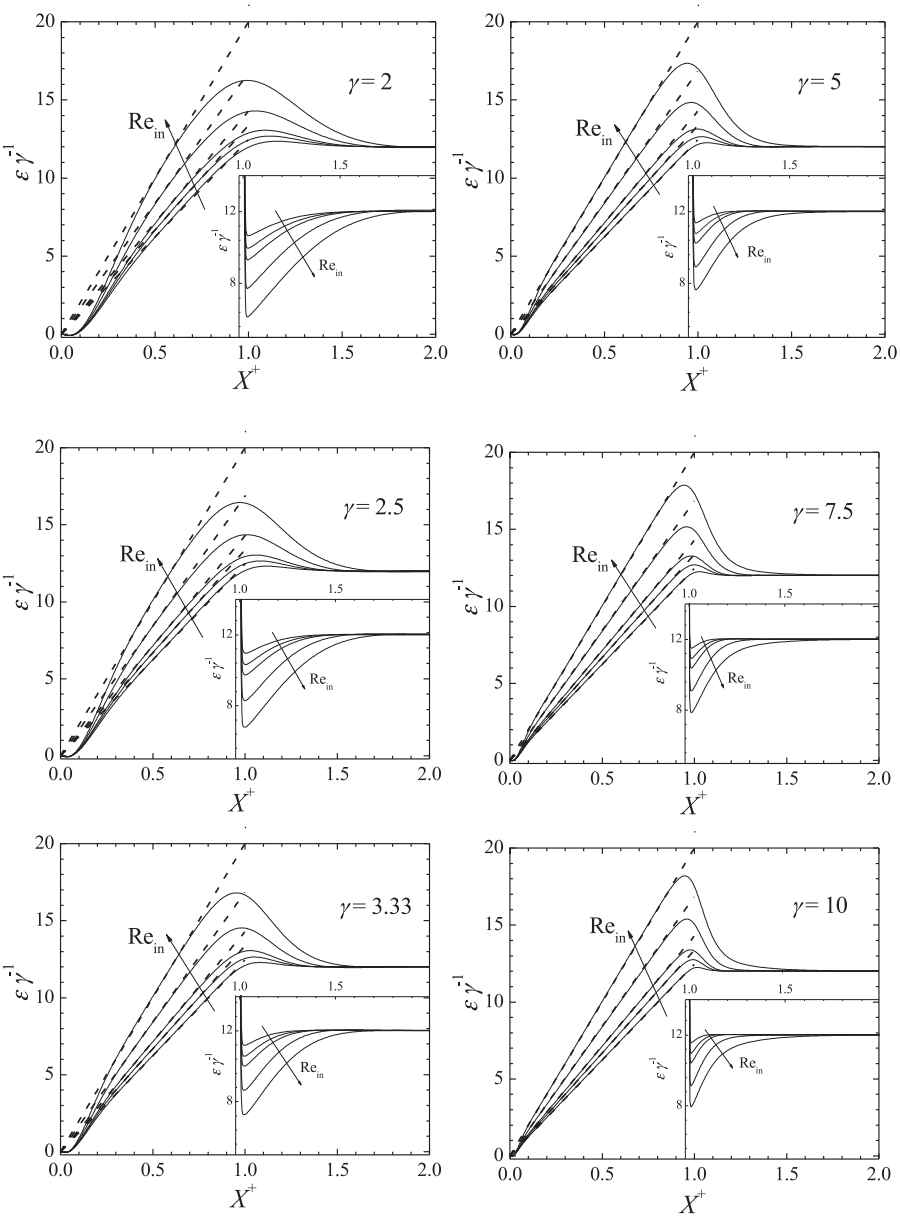

Fig. 4. Comparison of the slope in the velocity profile at the electrode surface as a function of the dimensionless axial position for different values of the aspect ratio γ and Reynolds numbers. Re_{in} = 1, 3, 5, 11 and 20. The arrows show the increase in Re_{in}. Full lines: numerical solutions of the Navier-Stokes equations. Dashed lines: solution according to Eq. (14). Inset: slope in the velocity profile at the counter electrode surface.

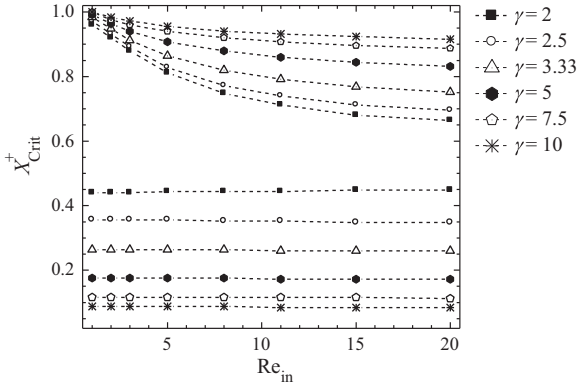

Fig. 5. Dimensionless entrance position, X^+, for which the relative deviation of ε according to the Navier-Stokes equations and Eq. (17) is 2% as a function of both the Reynolds number and the aspect ratio γ.

4.3. Mass-transfer performance

Fig. 7 shows typical curves of the experimental local mass-transfer coefficient as a function of the position along the electrode length, which are related to the data presented in Fig. 3. Each point represents the mean value of five independent experiments and the segments the standard deviation. Moreover, two theoretical calculations were performed. In the first, the local mass-transfer coefficient was computed according to Eq. (1) using a ε value obtained from the numerical resolution of the Navier-Stokes equations together with the continuity equation, Eqs. (9) to (11). In the second one, the OpenFOAM free software was used to calculate both the velocity and concentration profiles, using the simpleFoam routine and the scalarTransportFoam routine, respectively. The local mass-transfer coefficient along the electrode length was obtained from the slope of the concentration at the electrode surface. Additionally to the hydrodynamic boundary conditions above given, it

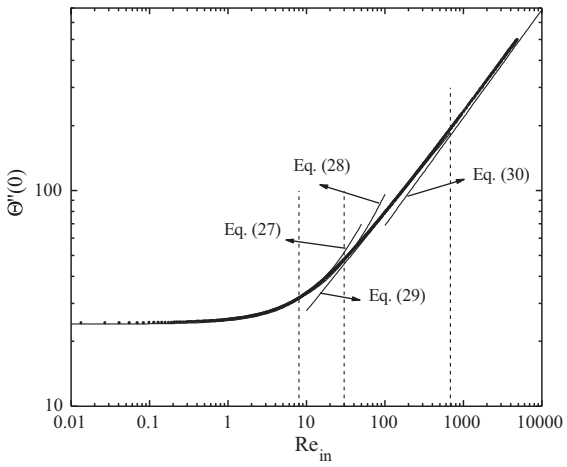

Fig. 6. $\Theta''(0)$ as a function of the Reynolds number. (○): according to Eq. (14). Full lines: limiting behaviours given by Eqs. (27) to (30).

was assumed that the concentration profile is uniform at the reactor inlet and the gradient of concentration is zero at the reactor outlet. The concentration was set to zero at the working electrode and the concentration gradients were null for the other solid walls. The absolute tolerance for the calculation of concentration profile was 1×10^{-6}. Further details about this rigorous numerical procedure are given in our previous paper [5]. No difference was observed between both numerical treatments, which are plotted as dashed lines in Fig. 7. Likewise, the full lines represent the theoretical behaviour for a parallel plate electrochemical reactor with infinitely wide electrodes and fully developed laminar flow, according to the following equation [19]

$$\mathrm{Sh_x} = 1.232\left(\frac{\mathrm{Re\,Sc}\,L}{x}\right)^{1/3} \tag{36}$$

being

$$\mathrm{Re} = \gamma \mathrm{Re_{in}} \tag{37}$$

here Re is the Reynolds number evaluated with the average fluid velocity inside the reactor. The inset compares dimensionless mass-transfer distributions. The symbols correspond to the experimental

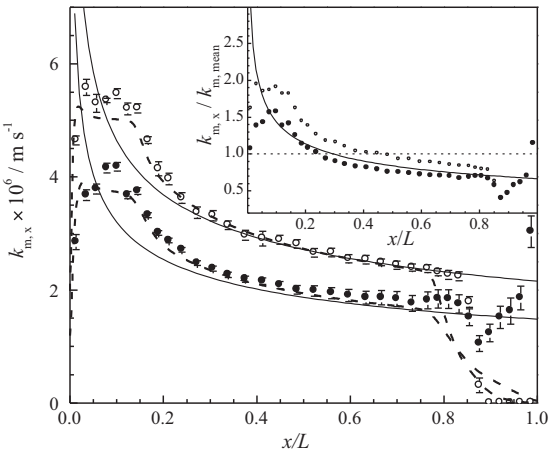

Fig. 7. Experimental local mass-transfer coefficient along the electrode length. Segments: standard deviation. (○): $d_h = 6.4$ mm, $\mathrm{Re_{in}} = 5.5$. and (●): $d_h = 10.8$ mm, $\mathrm{Re_{in}} = 9.35$. Full lines: theoretical prediction for a parallel plate electrochemical reactor with infinitely wide electrodes and fully developed laminar flow, from Eq. (36). Dashed lines: rigorous theoretical behaviour. Inset: dimensionless comparison of the experimental and theoretical mass-transfer distributions.

results, obtained as the ratio between the local mass-transfer coefficient and its mean value. The full line reports the dimensionless theoretical behaviour given by Eq. (36). It can be observed in Fig. 7 that the perpendicular inlet flow homogenizes the mass-transfer distribution at the entrance of the reactor and a monotonous decrease takes place along the electrode length. Likewise, the rigorous model approaches the experimental results in the inlet and central part of the reactor. The mass-transfer coefficient at the beginning of the electrode can be calculated by

$$\lim_{X\to 0} \mathrm{Sh_x} = \frac{1}{\Gamma\left(4/3\right)}\left[\frac{\mathrm{Re_{in}\ Sc}\,\varepsilon'(0)}{6}\right]^{1/3} \tag{38}$$

which was obtained applying the L'Hôpital's rule for $X \to 0$ to Eq. (1). At the reactor outlet, fluctuations are detected in the local mass-transfer coefficients which were strongly dependent on the type of experiment, corroborating that a perpendicular outlet flow is not convenient. For this reason the following discussion and comparison of experimental and theoretical results will be focused only half of the reactor including the perpendicular inlet of electrolyte.

Fig. 8 shows typical curves, for four hydraulic diameters, of the local Sherwood number as a function of the dimensionless axial position, X^+, for different values of the Reynolds number. The points correspond to experimental results and the full lines to Eq. (22), where $\Theta''(0)$ was obtained from Eqs. (27) to (30). Additionally, the results according to the rigorous numerical procedure are plotted as dashed lines. It can be observed in Fig. 8 an outstanding concordance between Eq. (22) and the rigorous theoretical treatment. The concordance between the results of both models is also appropriate for γ lower than 3 because the errors in the evaluation of ε using the simplified model are damped by Eq. (1). Likewise, there is a close agreement of the experimental points with both theoretical models. Fig. 8 also shows that a perpendicular and cumulative inlet flow homogenizes the mass-transfer distribution at the reactor inlet, which improves the performance of parallel-plate electrochemical reactors. The inset in Fig. 8 compares the primary current distribution, dashed line according to Eq. (35) normalized by its mean value, with the tertiary current distribution, full lines, obtained as the quotient between Eq (1) and its mean value along the electrode length for different Reynolds numbers. As expected, an important improvement in the uniformity of the current distribution is observed because of the effect of the mass-transfer. The primary distribution and the tertiary under limiting current conditions represent extreme behaviours and all the other cases, with different types of kinetic control, are between them.

Fig. 8 also makes it clear that the experimental and predicted local Sherwood numbers are in good qualitative agreement. To quantify the predictive capability of Eq. (22) with $\Theta''(0)$ according to Eqs. (27) to (30) the mean relative deviation, d_r, is introduced as

$$d_r = \frac{1}{N}\sum_{i=1}^{N}\frac{\left|\mathrm{Sh_{x,exp}}(x_i) - \mathrm{Sh_{x,Eq.(22)}}(x_i)\right|}{\mathrm{Sh_{x,Eq.(22)}}(x_i)} \tag{39}$$

being N the number of experimental points, 25. Fig. 9 displays the mean relative deviation between the experimental and theoretical results as a function of the Reynolds number for different values of the hydraulic diameter. The mean relative deviation ranges from 2.5% to 5%, which corroborates the good predictive capability of Eq. (22).

To determine the enhancement of the mass-transfer behaviour, the experimental results of mass-transfer are compared to those expected from a parallel plate electrochemical reactor with infinitely wide electrodes and fully developed laminar flow [5],

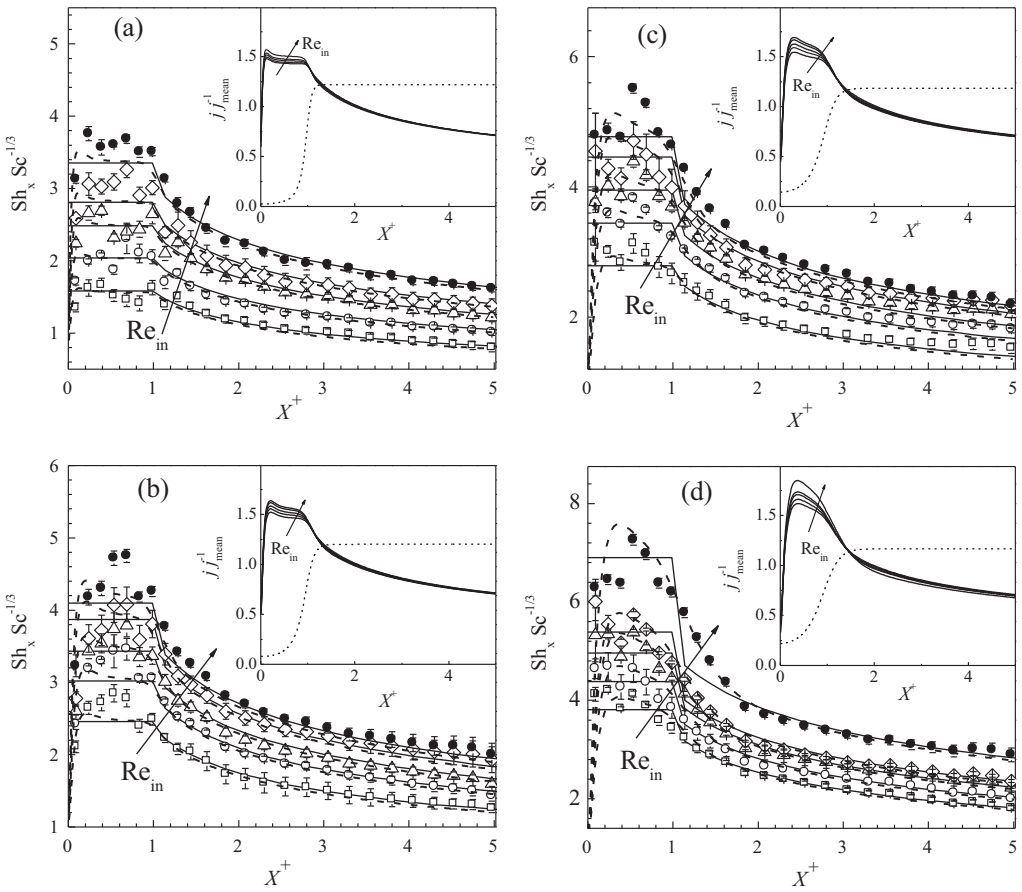

Fig. 8. Local Sherwood number as a function of the dimensionless position, X^+. Part (a): d_h = 6.4 mm, Re_{in} = 0.7, 1.44, 2.5, 3.5 and 5.5. Part (b): d_h = 10.8 mm, Re_{in} = 2.42, 4.22, 5.90, 7.95 and 9.35. Part (c): d_h = 15.2 mm, Re_{in} = 3.41, 5.94, 8.30, 11.20 and 13.16. Part (d): d_h = 19.6 mm, Re_{in} = 7.66, 10.70, 14.43, 16.97, and 29.90. Full lines: simplified theoretical behaviour according to Eq. (22). Dashed lines: rigorous theoretical behaviour. The arrows show the increase in Re_{in}. Inset: dashed line: primary current distribution. Full lines: tertiary current distribution.

Eq. (36), which represents the best mass-transfer distribution with axial inlet flow [18], and it is independent of the Reynolds number. Thus, Fig. 10 reports the uniformity factor defined as

$$UF = 1 - \frac{\delta_{mean}}{\delta_{mean}\,[Eq.(36)]} \tag{40}$$

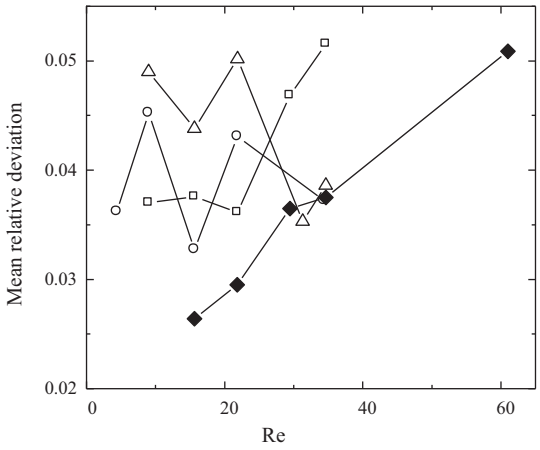

Fig. 9. Mean relative deviation between theoretical values, Eq. (22) and the experimental results as function of the Reynolds number. (○): d_h = 6.4 mm. (□):d_h = 10.8 mm. (△): d_h = 15.2 mm. (♦): d_h = 19.6 mm.

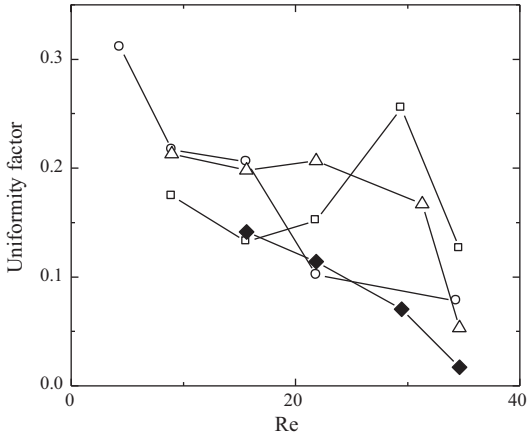

Fig. 10. Uniformity factor for mass-transfer distribution as a function of the Reynolds number. (○): d_h = 6.4 mm. (□):d_h = 10.8 mm. (△): d_h = 15.2 mm. (♦): d_h = 19.6 mm.

where δ_{mean} is given by

$$\delta_{mean} = \frac{1}{N}\sum_{1}^{N}\left|\frac{k_{m,x}}{k_{m,mean}} - 1\right| \tag{41}$$

According to Eq. (40) a positive value of UF means that the mass-transfer distribution in the reactor under study is more uniform than that given by Eq. (36) and negatives values are also possible.

The ideal case is UF = 1 when the distribution is totally uniform. Fig. 10 reports that, under laminar regime conditions, more uniform mass-transfer distributions are achieved with a perpendicular and cumulative inlet flow and the uniformity is enhanced when the Reynolds number decreases.

5. Conclusions

- Under laminar flow conditions, the use of a perpendicular and cumulative inlet flow makes uniform the mass-transfer in the reactor inlet.
- In electrochemical reactors with massive parallel-plate electrodes, the use of a perpendicular inlet flow requires that at the reactor inlet a portion of one electrode is not in front of the other producing an important primary current distribution, which is completely counteracted by the tertiary current distribution.
- The prediction of the mass-transfer behaviour according to a rigorous model involving computational fluid dynamics calculations shows an excellent agreement with the experimental results.
- A simplified theoretical model shows also a good concordance with the rigorous analytical model requiring lower computation time.
- The use of a perpendicular inlet flow represents a promising alternative to improve the performance of parallel-plate electrochemical reactors under laminar flow conditions.

Acknowledgements

This work was supported by the Agencia Nacional de Promoción Científica y Tecnológica (ANPCyT), Consejo Nacional de Investigaciones Científicas y Técnicas (CONICET) and Universidad Nacional del Litoral (UNL) of Argentina.

References

[1] Á. Frías-Ferrer, J. González-García, V. Sáez, C. Ponce de León, F.C. Walsh, The effects of manifold flow on mass transport in electrochemical filter-press reactors, AIChE Journal 54 (2008) 811.
[2] D. Pletcher, F.C. Walsh, Industrial Electrochemistry, 2nd ed., Chapman and Hall, London, 1993.
[3] I. Roušar, V. Cezner, Mass transfer coefficients and friction coefficients for rough electrodes, Institution of Chemical Engineers Symposium Series 98 (1986) 85.
[4] A. Shah, J. Jorne, Mass transfer under combined gas evolution and forced convection, Journal of the Electrochemical Society 136 (1989) 153.
[5] A.N. Colli, J.M. Bisang, Mass-transfer characterization in a parallel-plate electrochemical reactor with convergent flow, Electrochimica Acta 113 (2013) 575.
[6] J.O. Nanzer, A. Donizeau, F. Cœuret, Overall mass transfer between electrodes and normal impinging submerged multijets of electrolyte, Journal of Applied Electrochemistry 14 (1984) 51.
[7] J.O. Nanzer, F. Cœuret, Distribution of local mass transfer coefficients over one electrode bombarded by submerged multijets of electrolyte, Journal of Applied Electrochemistry 14 (1984) 627.
[8] Y. Oren, M. Abda, A. Tamir, Mass transfer in an electrochemical reactor with two interacting jets, Journal of Applied Electrochemistry 22 (1992) 950.
[9] G.W. Reade, C. Ponce de León, F.C. Walsh, Enhanced mass transport to a reticulated vitreous carbon rotating cylinder electrode using jet flow, Electrochimica Acta 51 (2006) 2728.
[10] P. Legentilhomme, J. Legrand, Overall mass transfer in swirling decaying flow in annular electrochemical cells, Journal of Applied Electrochemistry 20 (1990) 216.
[11] F.C. Walsh, G. Wilson, The electrolytic removal of gold from spent electroplating liquors, Transactions of the Institute of Metal Finishing 64 (1986) 55.
[12] S.A. Martínez-Delgadillo, H.R. Mollinedo P., M.A. Gutiérrez, I.D. Barceló, J.M. Méndez, Performance of a tubular electrochemical reactor, operated with different inlets, to remove Cr(VI) from wastewater, Computers and Chemical Engineering 34 (2010) 491.
[13] F. Cœuret, J. Legrand, Mass transfer at the electrodes of the 'falling-film cell', Journal of Applied Electrochemistry 15 (1985) 181.
[14] E. Erkoç, S. Yapici, B. Keskinler, A. Çakici, G. Akay, Effect of pulsed flow on the performance of carbon felt electrode, Chemical Engineering Journal 85 (2002) 153.
[15] J. Jorne, Mass transfer in laminar flow channel with porous wall, Journal of the Electrochemical Society 129 (1982) 1727.
[16] P. Lessner, J. Newman, Hydrodynamics and mass transfer in a porous-wall channel, Journal of the Electrochemical Society 131 (1984) 1828.
[17] J. Jorne, Flow distribution in the zinc-chloride battery, Journal of the Electrochemical Society 129 (1982) 2251.
[18] A.N. Colli, J.M. Bisang, Validation of theory with experiments for local mass transfer at parallel plate electrodes under laminar flow conditions, Journal of the Electrochemical Society 160 (2013) E5.
[19] D.J. Pickett, Electrochemical Reactor Design, 2nd ed., ELSEVIER, Amsterdam, 1979.
[20] A.S. Berman, Laminar flow in channels with porous walls, Journal of Applied Physics 24 (1953) 1232.
[21] H. Brown, B.B. Knapp, Nickel, in: F.A. Lowenheim (Ed.), Modern Electroplating, 3rd ed., John Wiley & Sons, New York, 1974, p. 287.
[22] O. Wein, K. Wichterle, Theory of segmented electrodiffusion probes: the effect of insulating insertions, Collection of Czechoslovak Chemical Communications 54 (1989) 3198.
[23] W.M. Taama, R.E. Plimley, K. Scott, Influence of supporting electrolyte on ferricyanide reduction at a rotating disc electrode, Electrochimica Acta 41 (1996) 549.
[24] A.N. Colli, PhD Thesis, Universidad Nacional del Litoral, 2013, http://bibliotecavirtual.unl.edu.ar:8180/tesis/handle/1/519?locale=en.